JMEPEG (2017) 26:6013–6021
https://doi.org/10.1007/s11665-017-3023-x

1059-9495/$19.00

The Effect of Grain Size on the Strain Hardening Behavior for Extruded ZK61 Magnesium Alloy

Lixin Zhang, Wencong Zhang, Wenzhen Chen, Junpeng Duan, Wenke Wang, and Erde Wang

(Submitted March 8, 2017; in revised form June 28, 2017; published online October 30, 2017)

The effects of grain size on the tensile and compressive strain hardening behaviors for extruded ZK61 alloys have been investigated by uniaxial tensile and compressive tests along the extrusion directions. Cylindrical tension and compression specimens of extruded ZK61 alloys with various sized grain were fabricated by annealing treatments. Tensile and compressive tests at ambient temperature were conducted at a strain rate of 0.5×10^{-3} s^{-1}. The results indicate that both tensile strain hardening and compressive strain hardening of ZK61 alloys with different grain sizes have an athermal regime of dislocation accumulation in early deformation. The threshold stress value caused dynamic recovery is predominantly related to grain size in tensile strain hardening, but the threshold stress values for different grain sizes are almost identical in compressive strain hardening. There are obvious transition points on the tensile strain hardening curves which indicate the occurrence of dynamic recrystallization (DRX). The tensile strain hardening rate of the coarse-grained alloy obviously decreases faster than that of fine-grained alloys before DRX and the tensile strain hardening curves of different grain sizes basically tend to parallel after DRX. The compressive strain hardening rate of the fine-grained alloy obviously increases faster than that of coarse-grained alloy for twin-induced strain hardening, but compressive strain hardening curves also tend to parallel after twinning is exhausted.

Keywords dynamic recovery, dynamic recrystallization, strain hardening, twinning, ZK61 alloy

1. Introduction

Magnesium alloys are possibly the lightest metals among the most commonly used metals, as well as with excellent physical properties including highly specific strength, high stiffness, and low density (Ref 1-3). Because of these attractive features, magnesium alloys have received considerable attention in applications ranging from automotive, aircraft, aerospace to automobile and computer, communication (3C) industries. However, the inherently poor formability of magnesium alloys at room temperatures, due to the limited number of slip systems in its hexagonal close packed (hcp) crystal structures, is a major obstacle for broadening the application fields of wrought Mg alloy products (Ref 4). In recent years, grain refinement is one of most well-known approaches to significantly strengthen the materials guided by the Hall–Petch relationship (Ref 5): $\sigma_{0.2} = \sigma_0 = kd^{-1/2}$ (where σ_0 is the frictional stress and k is the positive slope). Fine-grained microstructures have been proven to be favorable to strengthen magnesium alloys with better ductility by various severe plastic deformation (SPD) techniques, such as friction-stir processing (FSP) (Ref 6) and accumulative rolling bonding (ARB) (Ref 7). Unfortunately, although most of these SPD methods can be successfully applied to the magnesium alloys to obtain ultrafine-grained microstructures, the strong textures similar to those of the extruded-fiber and the rolled-plate would be introduced, resulting in significantly tension/compression asymmetry. The tension/compression asymmetry will restrict the application of magnesium alloys in those areas where the alloys are subjective to tension and compression simultaneously, especially for beams.

Although many efforts have been devoted to the investigation of yield behaviors, how to effectively improve the tension/compression yield asymmetry of Mg alloys by refining grains has not yet been fully resolved in recent years. The current study is designated to investigate the effects of the grain size on the tension and compression deformation mechanism and the tension/compression asymmetry in hot-extruded ZK61 alloys at room temperature. By studying the slope evolution of the strain hardening curves of the magnesium alloy rods with different sized grains in tension and compression, we try to reveal the primary causes of the tension/compression asymmetry.

2. Materials and Experimental Procedures

Extruded rods (with a diameter of ~ 36 mm) of a commercial grade ZK61 alloy (with a chemical composition of Mg-6.63wt.%Zn-0.56wt.%Zr) were used for this study. Specimens with a length of 70 mm were machined out of the extruded rod and then were annealed at 400 °C for 0.5, 2, 8, 24 and 48 h, respectively. The thermally treated specimens were sectioned

Lixin Zhang, School of Materials Science and Engineering, Harbin Institute of Technology, Weihai 264209, People's Republic of China and Department of Fundamental Experiment, Naval Aeronautical Engineering Institute, Yantai 264001, People's Republic of China; **Wencong Zhang, Wenzhen Chen, Wenke Wang,** and **Erde Wang**, Room A301, School of Materials Science and Engineering, Harbin Institute of Technology, Weihai 264209, People's Republic of China; and **Junpeng Duan**, Weihai Wangfeng Magnesium Industry Science and Technology Development Co. Ltd, Weihai 264209, People's Republic of China. Contact e-mail: zwinc@hitwh.edu.cn.

through the center parallel to the ED, polished and etched with an acetic parcel solution (10 ml acetic acid, 2 g picric acid, 70 ml ethanol, 10 ml water) for metallographic. Metallographic observation of the specimens was performed on an OLYMPUS GX71 optical microscopy (OM), and a linear intercept method was used to evaluate the grain size. Longitudinal sections at the same position in the specimens were prepared for x-ray diffraction (XRD) and electron backscattered diffraction (EBSD) measurements. XRD was performed on a D/Max-1200× diffractometry using Cu Kα radiation operated at 30 kV and 100 mA to compare the crystallographic orientation before and after the thermal treatment. EBSD was performed on a JEOL 733 electron probe equipped with TSL OIM analysis system to identify the textures of the extruded rods.

Mechanical properties of the annealed rods were examined by tension and compression at room temperature at a constant speed equal to an initial strain rate of 0.5×10^{-3} s^{-1}. The dimension of the specimens for tension was 6 mm in diameter and 15 mm in gauge length, while that for compression was 8 mm in diameter and 12 mm in length. The tension specimen and compression specimen were extracted from the annealed rods along the ED, as shown in Fig. 1.

3. Results and Discussion

Figure 2 displays the microstructural characteristics of the hot-extruded ZK61 alloy rods revealed by EBSD in the ED–TD (transverse direction) plane with the normal direction (ND) corresponding to the crystal reference system. The initial material contained recrystallization structures with an average grain size of 7.2 μm and exhibited intense extruded-fiber texture with {0002} basal plane parallel to the ED. The majority of the grain boundaries in the microstructures are high-angle grain boundaries (HAGs) with misorientation angles larger than 15°. A few {10-12} $< -1011 >$ tension twins are also observed, leading to a local peak at about 86° in the misorientation distribution map. The true strain–stress curves in Fig. 3(a) display two conspicuous curve shapes: a power-law curve in tension and a concave-down shape in compression, indicating the existence of obvious tension/compression asymmetry along the ED. It is clear that the ratio of the yield strength in tension to the yield strength in compression, commonly denoted as TYS/CYS, was about 1.4. The previous literatures

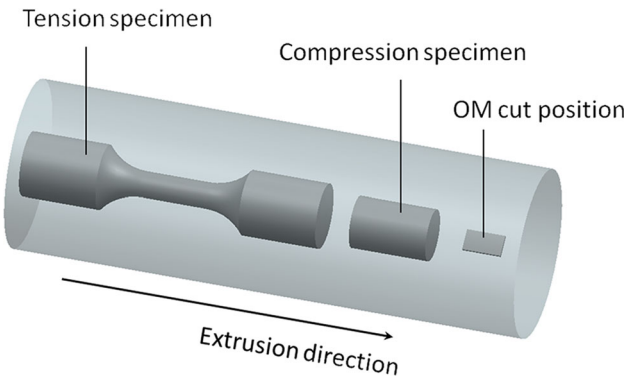

Fig. 1 Machining scheme of tension and compression specimens along the extrusion direction

indicate that the {10-12} twinning is not favored in tension but preferred in compression along the extrusion axis (Ref 8, 9). Thus, the yield asymmetry can be attributed to the prevalence of {10-12} twinning. To better represent the mechanical behavior, in-depth investigations on the strain hardening curves using $\theta - (\sigma - \sigma_{0.2})$ plot are shown in Fig. 3(b), where σ, ε and $\theta = d\sigma/d\varepsilon$ refer to stress, strain and strain hardening rate, respectively. A regime with a negative slope K_{sl} associated with the dynamic recovery was exhibited in tension, suggesting a continuous decrease in strain hardening rate ($d\theta/d\sigma < 0$). This means that the slip-dominated deformation dominated the most part of strain hardening in tension. The compression curve showed an increase in strain hardening rate at the early stage of deformation ($d\theta/d\sigma > 0$, denoted as K_{tw}), owning to the progressive reorientation of {10-12} tension twinning by 86°, with a steeper decrease after reaching a local maximum (point C, where twinning is exhausted) (Ref 8). This means that the slip-dominated deformation restarts to strain hardening in compression after twinning reaches saturation.

Figure 4 displays the optical microstructures obtained from longitudinal cuts in the center of the annealed ZK61 alloy rods. The grain sizes measured by a line intercept method are listed in Table 1. Figure 4(a) shows the as-extruded microstructure consists of a large amount of DRX grains with an average grain size of 7.2 μm. There are obvious grain flows along the ED. Numerous small recrystallization grains about 2 μm in size distribute mainly along the grain flows in the microstructures. There are very rare nucleation taking place in the ZK61 rods during subsequent isothermal annealing treatment; instead, the grains grow or merge to form large grains. Owing to the higher grain boundary energy in fine grain zones than in coarse grain zones, it can be seen from Fig. 4(b-f) that mobility of the grain boundary between small grains distributed along grain flows is higher than that of the other grains in the rods during the annealing process. Most of these fine grains merge into the strip grains at first, and then, the strip grains decompose into some small grains by static recrystallization processes. These small grains continue to grow up with the annealing time to achieve a homogeneous grain size distribution in the ZK61 rods after 48 h. The average grain size in the ZK61 alloy rods increases from 8.5 to 28.9 μm as the annealing time prolonged from 0.5 to 48 h.

To give insight into the texture evolution in the ZK61 alloy rods during the subsequent isothermal annealing treatments, the x-ray diffraction (XRD) characterization is employed. Figure 5 displays the XRD scans from the longitudinal sections at the same position of the as-extruded rod and the annealed rods at 400 °C for different times. The intensity of the (0002) peak (denoted as $I_{(1010)}/I_{(0002)}$ ratio) does not show observable change after annealing treatments, suggesting no evident change in orientations (Ref 10). Figure 6 shows {0002}, {10-10} and {11-20} pole figures of as-extruded rod and annealed rod at 400 °C for 48 h. The pole figures further confirm that the textures of the ZK61 alloy rods still remain an extruded-fiber texture with the basal planes parallel to the ED after annealing and only the density slightly decreases. This kind of texture hardly allows the existence of any twinning under tensile loading but of maximum twinning under compressive loading, which leads to tension/compression yield asymmetry of extruded ZK61 alloy rods (Ref 11, 12). After comparing the XRD scans of the as-extruded ZK61 alloy rod with that of the annealed ZK61 alloy rods carefully, it can be found that the as-

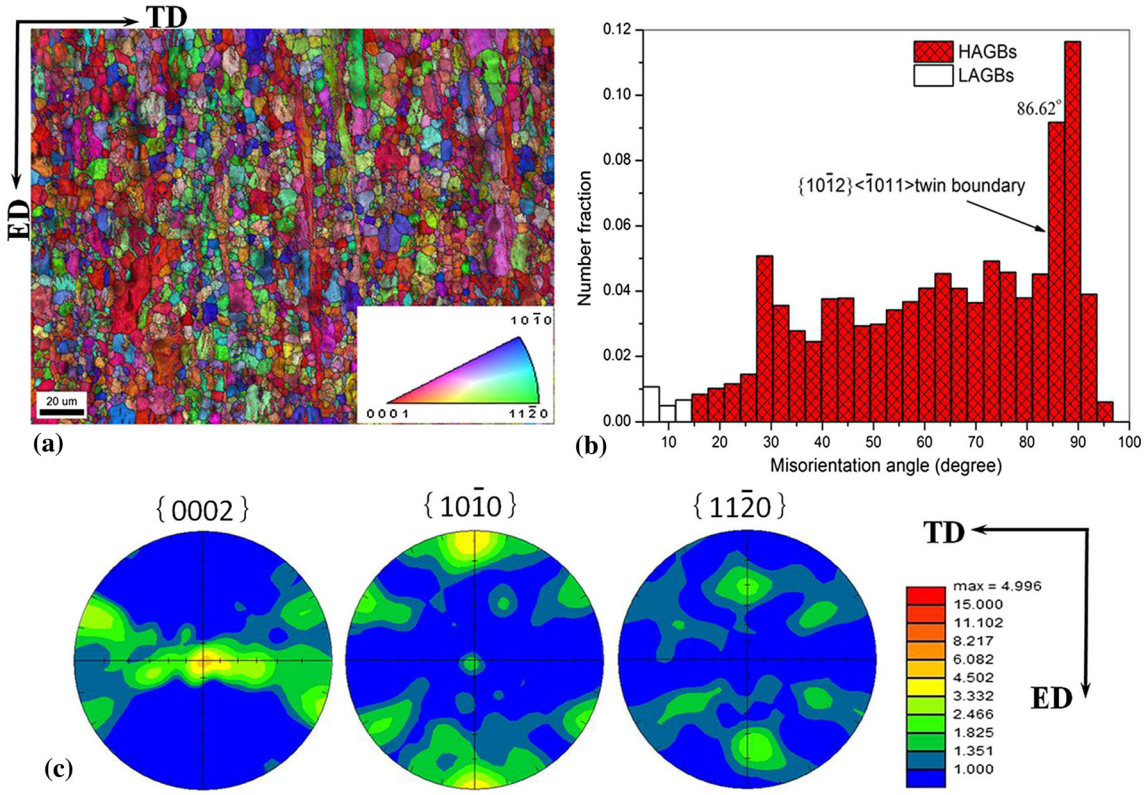

Fig. 2 Microstructural characteristics of as-extruded ZK61 alloy rods: (a) inverse pole figure map; (b) frequency vs. misorientation map (LAGBs low-angle grain boundaries with misorientation angles less than 15°, *HAGBs* high-angle grain boundaries with misorientation angles larger than 15°) and (c) {0002}, {10-10} and {11-20} pole figures

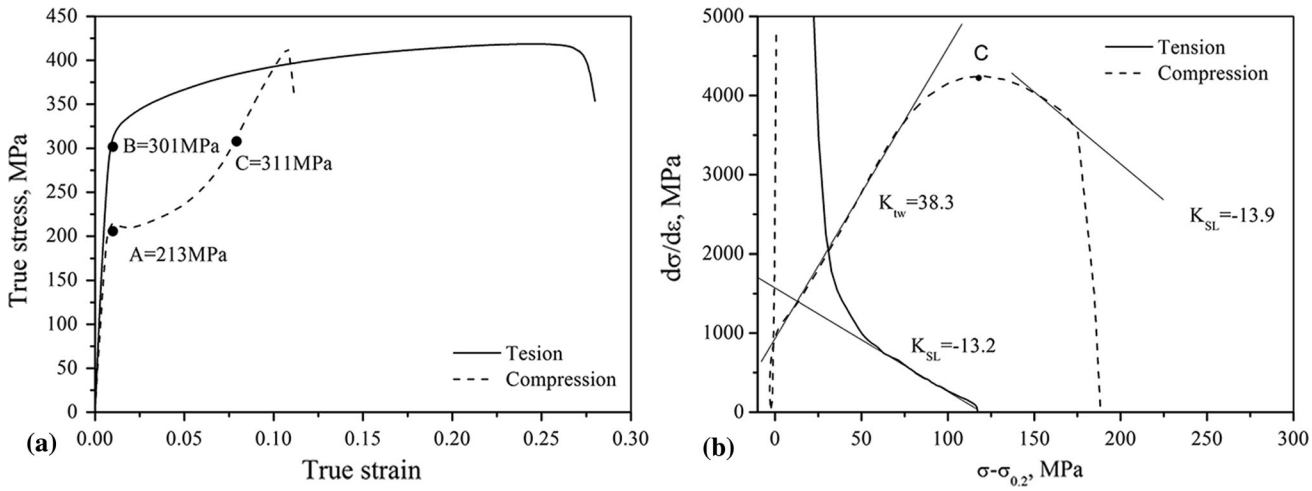

Fig. 3 Room-temperature mechanical behaviors for hot-extruded ZK61 alloy rods in tension and compression: (a) true stress–strain curve and (b) strain hardening curve using $\theta - (\sigma - \sigma_{0.2})$ plot

extruded ZK61 alloy rod contains a great number of precipitation phases of Mg-Zn compared to the annealed ZK61 alloy rods. These precipitated phases could affect the deformation mechanism and the mechanical properties of ZK61 alloy rods to some extent (Ref 13). However, here, we mainly focus on the effects of grain size on the deformation mechanism and the tension/compression yield asymmetry in extruded ZK61 alloys at room temperature, without considering the precipitated phases. Thus, we will not consider the as-extruded ZK61 alloy rod with a great number of precipitated phases of Mg-Zn in the following content.

The tension/compression asymmetry of the ZK61 alloy rods with different grain sizes could be clearly illustrated in the true stress–strain curves in tension and compression, as shown in Fig. 7. The date for the yield strength, the fracture strength and TYS/CYS in tension and compression are summarized in

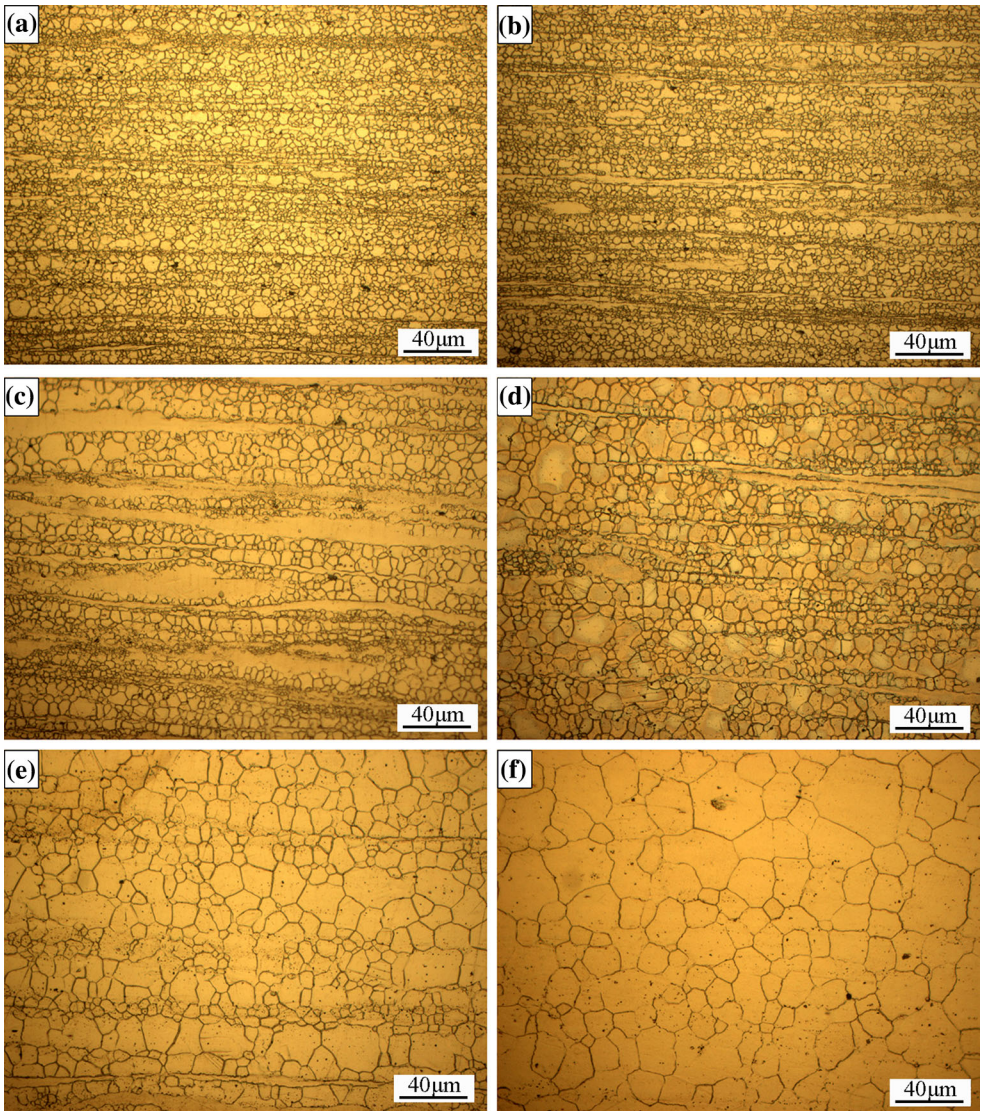

Fig. 4 Optical microstructures of the ZK61 alloy rods: (a) as-extruded and annealing-treated at 400 °C for (b) 0.5 h, (c) 2 h, (d) 8 h, (e) 24 h, (f) 48 h

Table 1 Grain sizes dependence on annealing time

Annealing time, h	0	0.5	2	8	24	48
Grain size, μm	7.2 ± 0.3	8.5 ± 0.2	9.2 ± 0.3	14.8 ± 0.4	22.8 ± 0.6	28.9 ± 0.2

Table 2. With the grain refining, the yield strength (0.2% in proof stress) increased monotonically in both tension and compression. The true strain–stress curves for different grain sizes in tension were still following power-law curves and the true strain–stress curves in compression remained concave-down shapes. These experimental phenomena indicate that the original deformation mechanism does not change in tension and compression with the grain coarsening during the annealing treatment. Strain hardening behavior is one of the important characteristic in the cold plastic deformation process of material at room temperature (Ref 14). Shown in Fig. 8, which are derived from Fig. 7, are the tensile and compressive strain hardening curves of ZK61 alloy with different grain sizes at room temperature. Figure 8(a) shows $d\sigma/d\varepsilon$ decrease sharply at lower net flow stress levels after tension yielding, but $d\sigma/d\varepsilon$ decrease slowly at higher net flow stress levels. There are obvious transition points on the tensile strain hardening curves between two stages. The linear stages of the tensile hardening curve at lower net flow stress levels and at higher net flow stress levels are noted as stage III and stage IV, respectively. The variation of strain hardening rate in the plastic deformation process of material is governed by a competition between hardening process and softening process. The strain hardening rate accounting for the recovery effects can be written as by as follows (Ref 15):

$$(\sigma - \sigma_{0.2})\Theta = (\sigma - \sigma_{0.2})\left[\Theta_h - \Theta_T\left(\sigma, \dot{\varepsilon}, T\right)\right]$$

where Θ is $d\sigma/d\varepsilon$; $\dot{\varepsilon}$ is the strain rate; T is the temperature; Θ_h is the athermal component of the strain hardening rate;

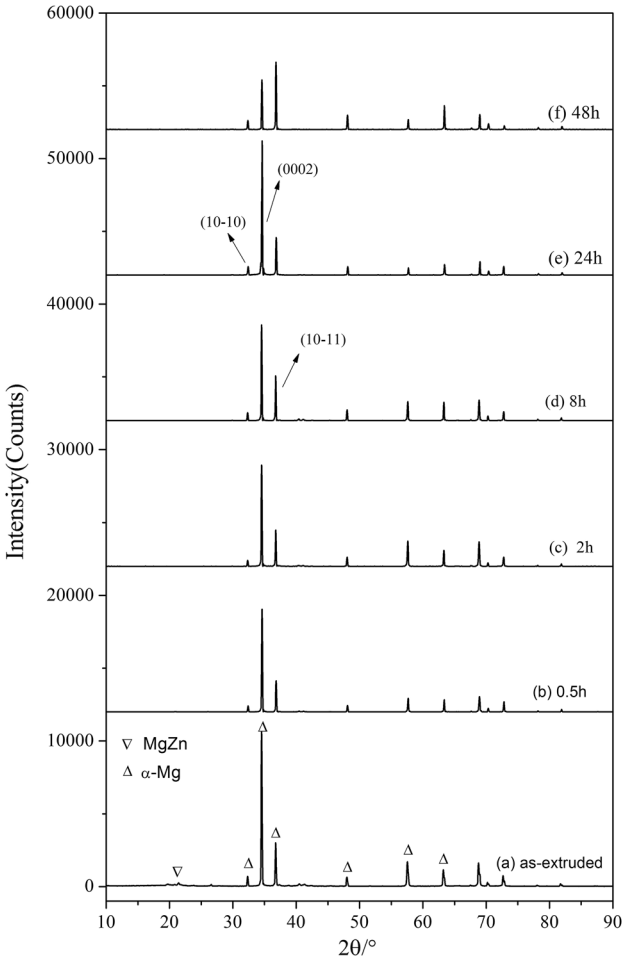

Fig. 5 XRD scans from the longitudinal planes of: (a) as-extruded rod, (b)-(f) annealing-treated rods at 400 °C for 0.5, 2, 8, 24 and 48 h, respectively

and Θ_T accounts for any softening effects due to dislocation annihilation by dynamic recovery as the temperature and/or the applied stress increases. In order to further investigate the evolution of the strain hardening rate depending on the net flow stress, we derived a plot of strain hardening rate Θ ($\sigma - \sigma_{0.2}$) versus net flow stress ($\sigma - \sigma_{0.2}$) from the strain hardening curves. Since we studied the strain hardening behavior of ZK61 alloys at room temperature and the same strain rate, we only considered the effect of stress on the softening of ZK61 alloy. Figure 8(c) shows the Θ ($\sigma - \sigma_{0.2}$) curves of ZK61 alloy with different grain sizes in tension. It can be seen that the initial tensile strain hardening curves of ZK61 alloy with different grain sizes can be fitted by straight lines passing through the origin, which are similar to those observed for FFC polycrystals (Ref 16). The slope Θ_h of these straight lines is almost same, but the extent of the linear region in the tensile strain hardening curves is depended on the grain sizes. A less extended linear hardening region Θ_h is visible for the larger grain. The related net flow stresses to the maximum values on the related Θ ($\sigma - \sigma_{0.2}$) curves are 38.9, 23.5 and 18.0 MPa for ZK61 alloy with grain sizes of 8.5, 14.8 and 28.9 μm, respectively. These results indicate that there is an athermal regime of dislocation accumulation before the softening for ZK61 alloy, and an earlier onset of dynamic recovery occurs for the larger grain. This is because grain boundaries in the ZK61 alloy with fine gains are obviously higher than those in the ZK61 alloy with large gains, and much higher activation energy is required for the plastic flow due to very stronger barriers to dislocation in the ZK61 alloy with fine gains. After dynamic recovery occurs, the Θ ($\sigma - \sigma_{0.2}$) tensile curves begin to decrease significantly and the corresponding tensile hardening curves segment exhibits a straight downward linear segment in Fig. 8(a). The slope K of these straight lines gradually increase with grain refinement, which indicates that ZK61 alloy with fine grains is more difficult to soften than that with large grains in the early stage of deformation. When the net flow stress ($\sigma - \sigma_{0.2}$) increases to a certain critical stress, the Θ ($\sigma - \sigma_{0.2}$) tensile curve exhibits an inflection point which indicates the onset of DRX (Ref 17). The inflection point is corresponding to the transition point on the tensile hardening curve between stage III and stage IV in Fig. 8(a). The corresponding net flow stresses at these transition points are 25.1, 62.0 and 68.5 MPa for ZK61 alloy with grain sizes of 8.5, 14.8 and 28.9 μm, respectively. When the deformation leads to the occurrence of DRX, the tensile strain hardening curve enters the stage IV and the slope K of the tensile strain hardening curves of different grain sizes basically tend to be uniform, $K = -16 \sim -18$. These results indicate that dynamic recovery due to the activation of the non-basal slip systems occurs in the early stage of softening and then followed by DRX (Ref 18). The threshold stress necessary to activate DRX is obviously lower for ZK61 with large grains than fine grains in tension at room temperature. However, the compressive strain hardening curves at room temperature show a trend completely different from the tensile strain hardening curves in Fig. 8(b) because the {10-12} twinning activity plays an important role at the start of compression deformation of the ZK61 alloys with extruded-fiber texture along the ED. The increase in the compressive strain hardening rate can be ascribed to effect of twin-induced grain reorientation to hard orientation and twin-induced introduction of barriers to dislocation movement (Ref 18). The previous studies (Ref 19, 20) have proved that the main contribution to increasing strain hardening rate come from texture strengthening, which rotates grain orientations into hard orientation due to {10-12} twinning. Thus, the compressive strain hardening rate of the ZK61 alloy with fine grains is obviously higher than that of coarse grains during the compression process because fine grains are favorable to rotate to hard orientation by {10-12} twinning. After reaching a local maximum at which twinning is exhausted, the compressive strain hardening curves tend to parallel, which means that the slip-dominated deformation begins to strain hardening in compression. Figure 8(d) shows the Θ ($\sigma - \sigma_{0.2}$) compressive curves of ZK61 alloy with different grain sizes can be fitted by straight lines and their slopes Θ_h are significantly less than that in tension at room temperature. With the increase in the net flow stress ($\sigma - \sigma_{0.2}$), Θ ($\sigma - \sigma_{0.2}$) compressive curves are gradually divided into the three separated curves. These results indicate that there is also an athermal regime of dislocation accumulation before hardening by twinning. The compressive hardening effect of ZK61 alloy with fine grains is stronger than that of ZK61 alloy with coarse grains. Figure 9 shows the SEM fracture morphologies of the extruded ZK61 alloy rods with 8.5 μm grain size. It can be observed from Fig. 9(a) that there exists evident tearing strips in the tension fracture morphologies whose distribution is intense yet uniform so that it can be classified into ductile frac-

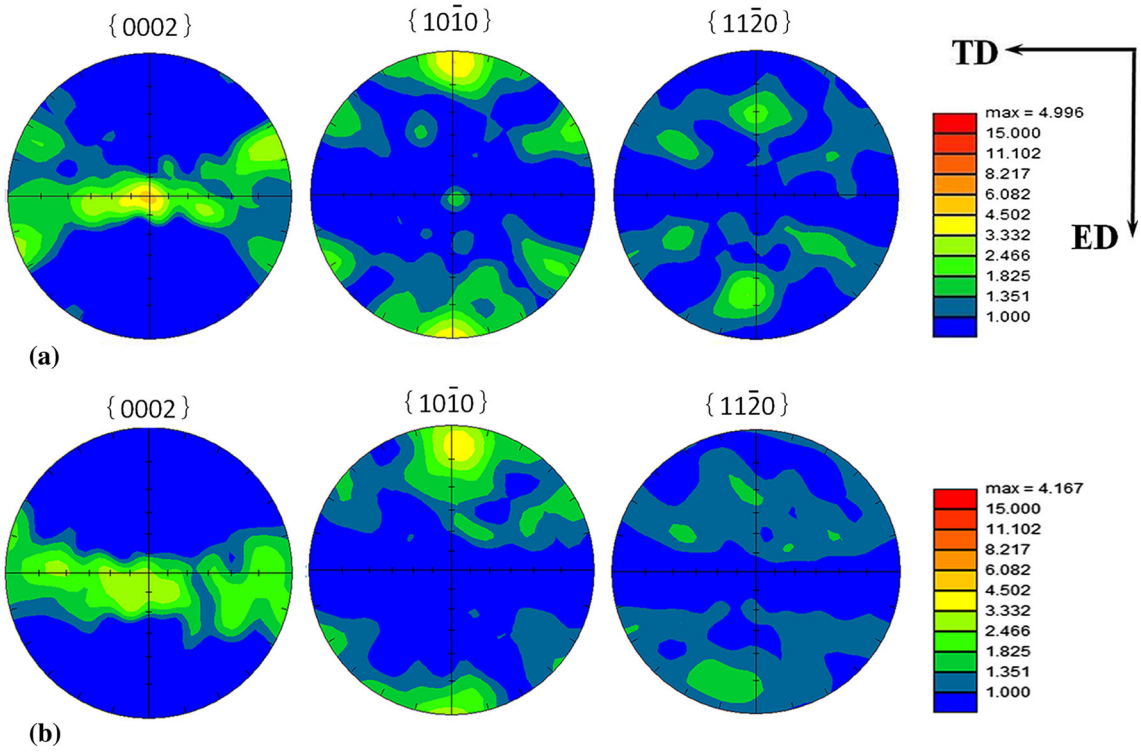

Fig. 6 {0002}, {10-10} and {11-20} pole figures of the ZK61 alloy rods: (a) as-extruded and (b) annealing-treated at 400 °C for 48 h

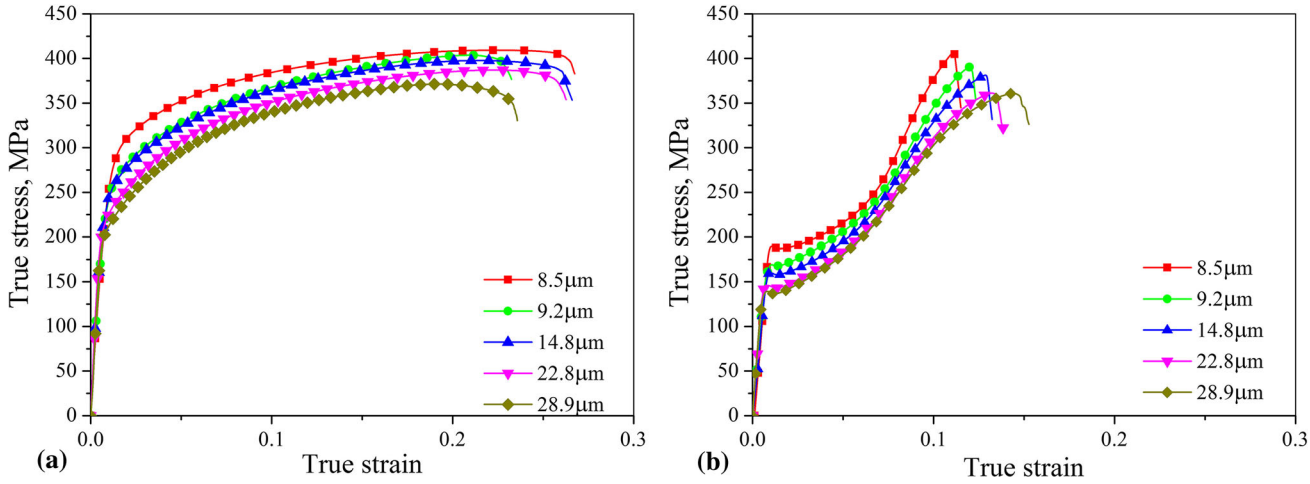

Fig. 7 Room-temperature true stress–true strain for ZK61 alloy rods with different grain sizes in tension (a) and compression (b)

Table 2 Summarized mechanical properties of the ZK61 magnesium alloy rods with different grain sizes

	YS, MPa		UTS, MPa		
Grain size, μm	**Ten.**	**Com.**	**Ten.**	**Com.**	**TYS/CS**
7.2 ± 0.3	301.0 ± 6.4	213.0 ± 6.5	359.3 ± 6.1	461.2 ± 8.1	1.41
8.5 ± 0.2	249.0 ± 6.9	191.5 ± 7.2	352.3 ± 12.4	455.3 ± 9.5	1.30
9.2 ± 0.3	223.2 ± 7.1	168.6 ± 7.5	342.9 ± 8.4	440.1 ± 10.3	1.32
14.8 ± 0.4	218.9 ± 7.6	161.3 ± 8.3	339.3 ± 13.5	433.9 ± 12.5	1.36
22.8 ± 0.6	204.9 ± 7.3	147.2 ± 7.7	327.9 ± 10.1	412.7 ± 13.3	1.39
28.9 ± 0.2	197.7 ± 6.4	138.5 ± 5.8	318.9 ± 11.8	417.4 ± 6.3	1.43

YS yield strength, *UTS* ultimate strength, *TYS*/*CYS* ratio of YS between tension and compression

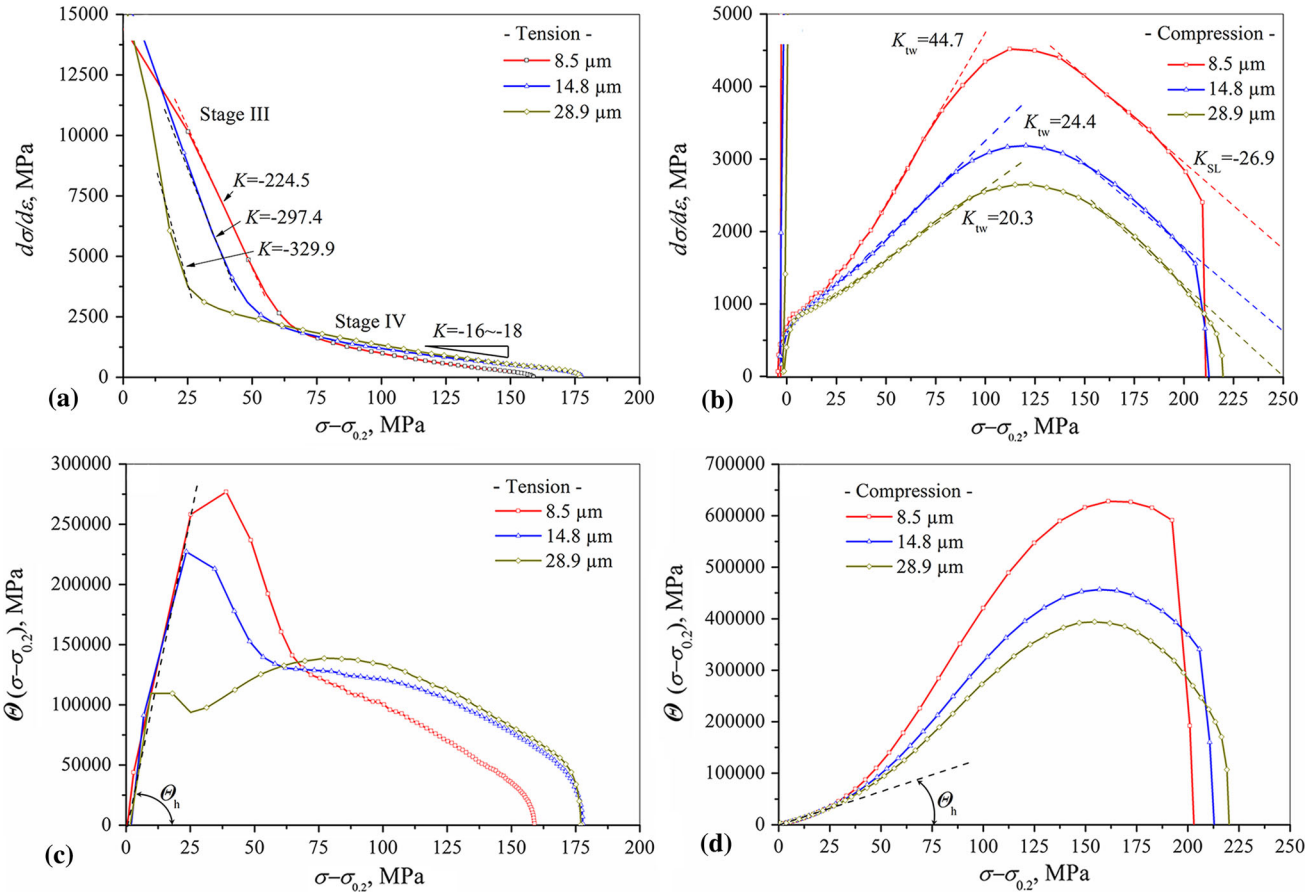

Fig. 8 Effects of different grain sizes on room-temperature strain hardening of ZK61 alloy rods: Θ vs. $(\sigma - \sigma_{0.2})$ plot in tension (a) and compression (b) and Θ $(\sigma - \sigma_{0.2})$ vs. $(\sigma - \sigma_{0.2})$ plot in tension (c) and compression (d)

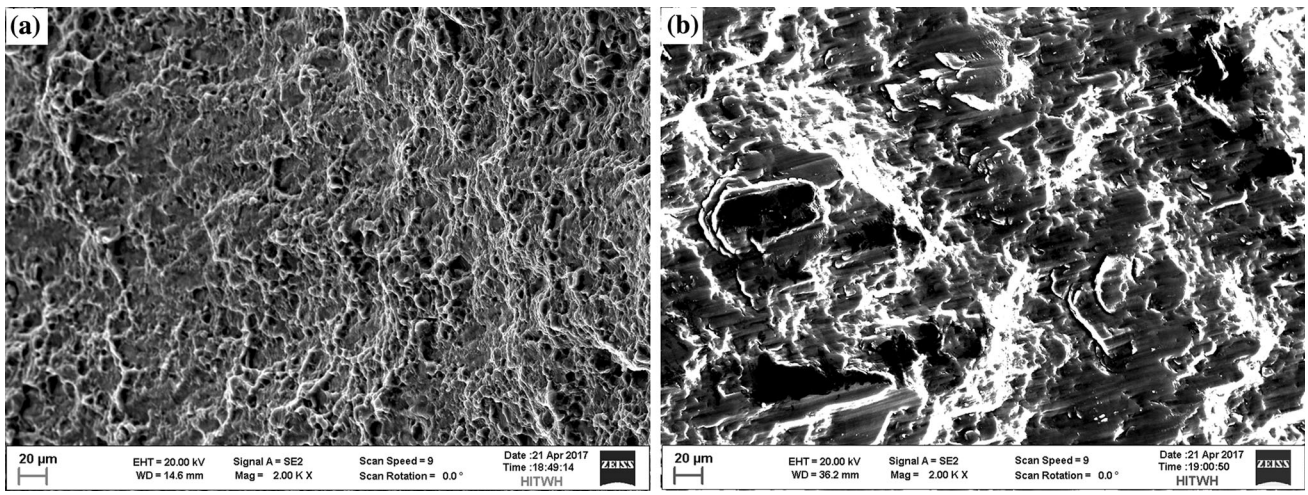

Fig. 9 SEM fracture morphologies of the ZK61 alloy rod with 8.5 μm grain size in tension (a) and in compression (b)

ture. In Fig. 9(b), in the compression fracture morphologies emerge apparent tearing strips with cleavage planes and cleavage steps; hence, it belongs to tough and brittle-type quasi-cleavage fracture. Neglecting the effect of precipitations on the strength, Fig. 10 shows the variation of strengths of the ZK61 alloy rods as a function of the grain size in tension and compression, respectively. It can be seen that the yield strength increases as the grain size decreases for both tension and compression, which can be described by the Hall–Petch relationship: $\sigma_{0.2} = \sigma_0 = kd^{-1/2}$, where σ_0 is the frictional stress for dislocation movement. The slope of k depends on the orientation relation between the interacting grains and the critical shear stresses of the activated deformation modes in both grains. The extruded-fiber texture of the ZK61 alloy rods during annealing treatments can be roughly deemed as unchanged, as discussed above. This means no prominent

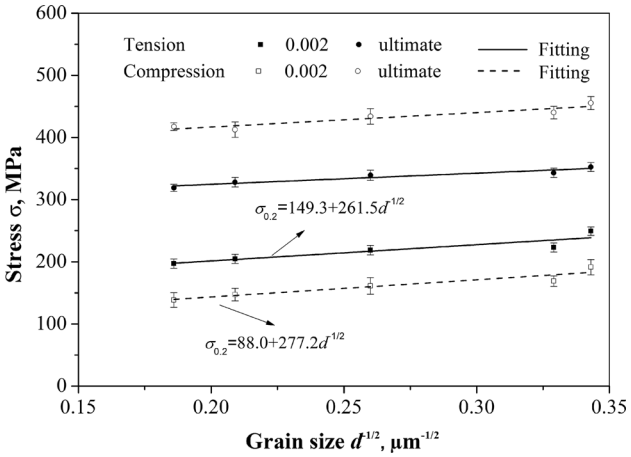

Fig. 10 Hall–Petch relationship for the ZK61 alloy rods with different grain sizes in tension and compression

change in the orientation relation between the interacting grains under the annealing condition. Therefore, the slope of k mainly depends on the critical shear stresses of the activated deformation modes in both tension and compression processes. Although the grain size in the tension samples is the same as in the compression samples, they have different deformation mechanisms. Slip of dislocations dominates the tension deformation along ED and must be hindered by the increased number of grain boundaries caused by the grain refining with the result that the yield strength of tension increases. Twinning dominates the compression deformation along ED and is prone to occur in the samples with large grains (Ref 21, 22). Therefore, the twinned regions in the compression deformation material decrease gradually with grain refining, and eventually slip of dislocations gradually dominates the deformation once again. In the pure magnesium single crystals, the critical resolved shear stress (CRSS) for {10-12} twinning is approximately 4 MPa and that for prismatic slip is approximately 40 MPa (Ref 23). This obvious difference leads to the fact that the compression yield strength of the ZK61 alloys with coarse grains is lower than that of the ZK61 alloys with fine grains, resulting in the decreased tension/compression asymmetry with the grain refining. But Fig. 10 shows that the Hall–Petch slopes of tension and compression are not visibly different and the slope of tension is 261.5 and that of compression is 277.2. Table 2 also indicates the TYS/CYS of the extruded ZK61 alloy merely decreases from 1.43 of 28.9 μm to 1.30 of 8.5 μm. Therefore, the grain size hardly affects the tension/compression asymmetry of extruded ZK61 alloy rods in the grain size range from 28.9 to 8.5 μm. Although Yin et al. (Ref 24) have shown that the tension/compression yield asymmetry of ZK31 magnesium alloy rods has nothing to do with their textures when their grains are as small as to be about 0.8 μm, it is very difficult to refine the magnesium alloy grains to about 0.8 μm by purely using the conventional extrusion. Even possible, it will increase the cost substantially. Thus, the grain refinement is not an economic and practical technique method to improve the tension/compression yield asymmetry of ZK61 alloy rods. The most efficient way to improve the mechanical asymmetry in the tension and compression processes is to suppress the twinning during compression by weakening the texture or by adding rare earth elements into the magnesium alloys.

4. Conclusions

The room-temperature strain hardening behaviors of the extruded ZK61 rods owning a similar extruded-fiber texture but different grain sizes in the range from 8.5 to 28.9 μm have been studied by uniaxial tensile and compressive tests in this study, and several conclusions are summarized as follows:

1. Both tensile strain hardening and compressive strain hardening of ZK61 alloy with different grain sizes have an athermal regime of dislocation accumulation in early deformation. The slopes Θ_h of the Θ $(\sigma - \sigma_{0.2})$ compressive strain hardening curves are significantly less than that of the Θ $(\sigma - \sigma_{0.2})$ tensile strain hardening curves.
2. The threshold stress value of dynamic recovery for the ZK61 alloy with coarse grains is significantly less than that of the ZK61 alloy with fine grains in tensile strain hardening, but the threshold stress values of twinning hardening for different grain sizes are almost identical in compressive strain hardening.
3. The hardening effect of ZK61 alloy with fine grains is stronger than that of ZK61 alloy with coarse grains for both tensile strain hardening and compressive strain hardening on the early stages. The tensile strain hardening curves of different grain sizes basically tend to be parallel after DRX, and the compressive strain hardening curves tend to parallel after twinning is exhausted.

Acknowledgments

This work was supported by National Natural Science Foundation of China (Grant No. 51401064), Sci-tech Development Project in Shandong Province (Grant No. 2014GGX10211) and Sci-tech Major Project in Shandong Province (Grant No. 2015ZDJQ02002).

References

1. H. Takuda, T. Enami, K. Kubota, and N. Hatt, The Formability of a Thin Sheet of Mg-8.5Li-1Zn Alloy, *J. Mater. Process. Technol.*, 2000, **101**(1-3), p 281-286
2. J.A. del Valle, M.T. Pérez-Prado, and O.A. Ruano, Texture Evolution During Large-Strain Hot Holling of the Mg AZ61 Alloy, *Mater. Sci. Eng., A*, 2003, **355**(1-2), p 68-78
3. J. Bohlen, S.B. Yi, J. Swiostek, and D. Letzig, Microstructure and Texture Development During Hydrostatic Extrusion of Magnesium Alloy AZ31, *Scr. Mater.*, 2005, **53**(2), p 259-264
4. H. Watanabe and K. Ishikawa, Effect of Texture on High Temperature Deformation Behavior at High Strain Rates in a Mg-3Al-1Zn Alloy, *Mater. Sci. Eng., A*, 2009, **523**(1-2), p 304-311
5. A. Jain, O. Duygulu, and D.W. Brown, Grain Size Effects on the Tensile Properties and Deformation Mechanisms of a Magnesium alloyAZ31B Sheet, *Mater. Sci. Eng., A*, 2008, **486**(1-2), p 545-555
6. W. Woo, H. Choo, and D.W. Brown, Texture Variation and Its Influence on the Tensile Behavior of a Friction-Stir Processed Magnesium Alloy, *Scr. Mater.*, 2006, **54**(11), p 1859-1864

7. M.T. Pérez-Prado, J.A. del Valle, and O.A. Ruano, Achieving High Strength in Commercial Mg Cast Alloys Through Large Strain Rolling, *Mater. Lett.*, 2005, **59**(26), p 3299-3303
8. X.Y. Lou, M. Li, R.K. Boger, and R.H. Wagoner, Hardening Evolution of AZ31B Mg Sheet, *Int. J. Plast.*, 2007, **23**(1), p 44-86
9. Marko Knezevic, Amanda Levinson, and Ryan Harris, Deformation Twinning in AZ31: Influence on Strain Hardening and Texture Evolution, *Acta Mater.*, 2010, **58**(19), p 6230-6242
10. Y.N. Wang and J.C. Huang, The Role of Twinning and Untwining in Yielding Behavior in Hot-Extruded Mg-Al-Zn Alloy, *Acta Mater.*, 2007, **55**(3), p 897-905
11. E.A. Ball and P.B. Prangnell, Tensile-Compressive Yield Asymmetries in High Strength Wrought Magnesium Alloys, *Scr. Metal. Mater.*, 1994, **31**(2), p 111-116
12. M.R. Barnett, C.H.J. Davies, and X. Ma, An Analytical Constitutive Law for Twinning Dominated Flow in Magnesium, *Scr. Mater.*, 2005, **52**(7), p 627-632
13. J.F. Nie, Preface to Viewpoint Set on: Phase Transformations and Deformation in Magnesium Alloys, *Scr. Mater.*, 2003, **48**(8), p 981-984
14. X.H. Chen and L. Lu, Work Hardening of Ultrafine-Grained Copper with Nanoscale Twins, *Scr. Mater.*, 2007, **57**(2), p 133-136
15. N. Afrin, D.L. Chen, X. Cao, and M. Jahazi, Strain Hardening Behavior of Friction Stir Welded Magnesium Alloy, *Scr. Mater.*, 2007, **57**(11), p 1004-1007
16. U.F. Kocks and H. Mecking, Physics and Phenomenology of Strain Hardening: The FCC Case, *Prog. Mater Sci.*, 2003, **48**(3), p 171-273
17. H.Y. Wu and F.Z. Lin, Mechanical Properties and Strain-Hardening Behavior of Mg Alloy AZ31B-H24 Thin Sheet, *Mater. Sci. Eng., A*, 2010, **527**(4-5), p 1194-1199
18. B.S. Wang, R.L. Xin, G.J. Huang, and Q. Liu, Effect of Crystal Orientation on the Mechanical Properties and Strain Hardening Behavior of Magnesium Alloy AZ31 During Uniaxial Compression, *Mater. Sci. Eng., A*, 2012, **2012**(534), p 588-593
19. M.R. Barnett, Z. Keshavarz, A.G. Beer, and D. Atwell, No-Schmid Behavior During Secondary Twinning in a Polycrystalline Magnesium Alloy, *Acta Mater.*, 2008, **52**(1), p 5093-5103
20. M. Knezevic, A. Levinson, R. Harris, and R.K. Mishra, Deformation Twinning in AZ31: Influence on Strain Hardening and Texture Evolution, *Acta Mater.*, 2010, **58**(19), p 6230-6242
21. M.A. Meyers, O. Vöringer, and V.A. Lubarda, The Onset of Twinning in Metals: A Constitutive Description[J], *Acta Mater.*, 2001, **49**(19), p 4025-4039
22. S.R. Agnew, M.H. Yoo, and C.N. Tomé, Application of Texture Simulation to Understanding Mechanical Behavior of Mg and Solid Solution Alloys Containing Li or Y, *Acta Mater.*, 2001, **49**(20), p 4277-4289
23. E.W. Kelley and W.F. Hosford, Plane-Strain Compression of Magnesium and Magnesium Alloy Crystals, *Trans. Met. Soc. AIME*, 1968, **242**(1), p 5-13
24. S.M. Yin, C.H. Wang, and Y.D. Diao, Influence of Grain Size and Texture on the Yield Asymmetry of Mg-3AL-1Zn Alloy, *J. Mater. Sci. Technol.*, 2011, **27**(1), p 29-34